Identifying the hygroscopic properties of fine aerosol particles from diverse sources in urban atmosphere and the applicability in prediction of cloud nuclei

Jingye Ren [a,b], Fang Zhang [b,*], Lu Chen [a], Gang Cao [b], Mengyu Liu [b], Xue Li [a], Hao Wu [c], Yiling Cheng [b], Zhanqing Li [d]

[a] *College of Global Change and Earth System Science, Beijing Normal University, Beijing, 100875, China*
[b] *School of Civil and Environmental Engineering, Harbin Institute of Technology (Shenzhen), 518055, Shenzhen, China*
[c] *Key Laboratory of China Meteorological Administration Atmospheric Sounding, School of Electrical Engineering, Chengdu University of Information Technology, Chengdu, 610225, China*
[d] *Earth System Science Interdisciplinary Center, Department of Atmospheric and Oceanic Science, University of Maryland, College Park, College Park, MD, USA*

HIGHLIGHTS

- The hygroscopicity of aerosol particles from specific sources was identified in winter of Beijing.
- The hygroscopic growth factors together with aerosol spectrum could predict N_{CCN} well at typical supersaturation in cloud.
- Secondary sources were the dominant contributor to the total cloud nuclei, while primary particles contributed less.

ARTICLE INFO

ABSTRACT

Aerosols hygroscopicity is generally differentiating for particles among various sources, leading to complex effects on visibility impairment and cloud formation. However, the hygroscopicity of aerosol particles from diverse sources is not yet fully understood. Here, combining field observations at an urban site in Beijing and a positive matrix factorization model, we identified aerosols hygroscopicity of six different sources, nucleation, traffic, cooking, aging primary, residential heating, and regional secondary, which corresponds to hygroscopic growth factors (Gfs) of 1.23, 1.15, 1.17, 1.44, 1.48, and 1.47, respectively at relative humidity of 90%. On polluted days, Gf values of particles for the accumulation-mode particles were higher than that under clean conditions. This is largely due to the hygroscopic sources represented by aged and secondary processes showed the dominant role in aerosol population. While on clean days, the Gfs of 40-nm particles showed larger values, that is closely associated with the photochemical-nucleation-sourced particles. By further applying the Gfs together with aerosol spectrum to predict cloud nuclei concentration (CCN), we find the predicted and observed CCN number concentration are well correlated at typical supersaturation in cloud. The study further reveals the dominant roles of secondary processes, contributing up to 90% of the total cloud nuclei. Primary particles from traffic/cooking activities contributed only ~5%, although they account for 30–40% of the total particle number concentrations in urban Beijing during the studied period. The results indicate the source apportionment of Gfs can well interpret the variation in hygroscopicity of aerosols under different atmospheric conditions and evaluate their effects on cloud formation.

1. Introduction

Aerosol hygroscopicity is a vital parameter to assess the changes of atmospheric visibility (Liu et al., 2020; Xu and Kuang, 2020) and its effects on climate change (Kandler and Schütz, 2007; Wu and Poulain, 2013). It describes the water uptake capacity of particles with the relative humidity increasing and have important implications in understanding aerosol phy-chemical properties during atmospheric

processes (Vu et al., 2015; Swietlicki et al., 2008) and aerosol direct and indirect climate effects (Massoli et al., 2009; Wang and Chen, 2019). Aerosol particle sizes and compositions significantly change when absorbing water vapor, modifying their optical properties, and directly affecting visibility and air quality (Bäumer et al., 2008; Zhao and Hu, 2022) and the radiative balance (Cheng et al., 2008). Furthermore, aerosol hygroscopicity is also directly linked to cloud condensation nuclei (CCN) activity, thus affecting microphysical structures and radiative properties of clouds (Petters and Kreidenweis, 2007; Rosenfeld et al., 2017).

The characteristics of aerosol hygroscopicity can be measured using the hygroscopic tandem differential mobility analyzer (HTDMA) system. The hygroscopic growth factor (Gf) is one of the most widely used parameters describing the hygroscopic properties of aerosols (Swietlicki et al., 2008; Petters and Kreidenweis, 2007). The hygroscopicity properties of ambient aerosols are determined by physical and chemical properties, such as size, physical state, morphology, and chemical composition (Swietlicki et al., 2008; Mikhailov et al., 2009). Existing measurement techniques cannot directly distinguish the hygroscopic properties of particles from different sources. To date, focus has been placed on the bulk Gfs of ambient aerosol particles based on field measurements (Cai et al., 2018; Fan et al., 2020) and laboratory studies (Martin et al., 2013; Li et al., 2019; Zhang et al., 2022). Aerosols emitted from different sources may have distinct hygroscopic properties due to the diversity in size and chemical composition. For example, Swietlicki et al. (2008) reviewed aerosol hygroscopic properties from various environments and investigated how their chemical and physical properties affected hygroscopic growth. The hygroscopicity of particles emitted from traffic emissions or burning sources may both be related to the type of fuel, the combustion process, and the aging process (Happonen et al., 2013; Martin et al., 2013). Most of these previous studies are concerned with the relationship between aerosol hygroscopicity and chemical composition. Particles emitted into atmosphere would change their size and hygroscopicity under the influence of the aging processes (eg., condensation, coagulation and other phy-chemical processes). To date, the heterogeneity of the hygroscopic properties among different sources is still poorly understood in ambient atmosphere. Separating the hygroscopic growth factors is capable of providing an insight in application of evaluating visibility and air quality. It is thus critical to characterize the hygroscopic properties of aerosol particles from different sources.

In addition, identifying the hygroscopic properties of particles from various sources is important for accurately assessing their climate effects. A general application of the derived Gfs is still lacking. For example, its application in CCN prediction, which still incurs large uncertainties in polluted regions, would help improve the characterization and parameterization of CCN activation. To our knowledge, most previous CCN closure studies conducted in China were based on the application of particle number size distribution (PNSD) and bulk hygroscopicity to calculate CCN number concentrations (N_{CCN}) (Zhang et al., 2017; Ren et al., 2018). The properties of ambient particles may be difficult to estimate using a single bulk hygroscopic parameter due to the complexity of the physical and chemical characteristics. This indicates the importance of using hygroscopic properties of aerosols from various sources in the calculation of N_{CCN}. In order to accurate parameterize CCN, it is necessary to explore the characteristics of hygroscopic property of specific sources, especially in those regions where the aerosol particles are affected by multiple source types.

In this study, a positive matrix factorization (PMF) model was applied to identify the hygroscopic growth properties of fine aerosol particles from different sources in urban Beijing using PNSDs and probability distributions of the growth factor (Gf-PDF) observed during the winter of 2016. The identified Gfs were then compared with those reported in the literature. The Gfs were further applied to estimate N_{CCN} combined with PNSDs measured in another field campaign that took place in urban Beijing in 2014. The contribution of aerosol particles from different sources to the N_{CCN} in urban Beijing during the study period was evaluated.

2. Methods

2.1. Experiment and data

Two in-situ measurement campaigns were conducted at an urban site in Beijing, located at the Institute of Atmospheric Physics (39.97°N, 116.37°E). The field campaigns were carried out in winter: from 7 November to 17 December in 2014 and from 16 November to 10 December in 2016. Here, a brief introduction is given here on the aerosol sampling and data analysis performed in this study. Xu et al. (2019) and Zhang et al. (2019) provide detailed descriptions about the operation of the instruments and data calibrations.

The key instrument in the two field campaigns was the scanning mobility particle sizer (SMPS; Wang et al., 1990). Briefly, ambient particles larger than 1 µm were first removed by a sharp-cut particulate. Sampled particles were then introduced into a bundled Nafion dryer to ensure that the relative humidity (RH) of the flow was below 30%. The PNSDs were measured using two SMPSs, each equipped with a differential mobility analyzer (DMA, model 3081, TSI Inc.) and a condensation particle counter (models 3762 in 2014 and 3775 in 2016, TSI Inc.). Particles in the 16–560 nm (the 2014 field campaign) and 10–550 nm (the 2016 field campaign) size ranges were measured at an interval of 5 min. An HTDMA system was used in 2016 to measure the hygroscopic growth factor of five selected diameters (40, 80, 110, 150, and 200 nm) at a given RH (90%). The Gf-PDF was retrieved based on the TDMAinv algorithm (Gysel et al., 2009). In addition, non-refractory aerosol species, including organics (Org), sulfate (SO_4), nitrate (NO_3), ammonium (NH_4), and chloride, were measured by an Aerodyne high-resolution time-of flight aerosol mass spectrometer (HR-AMS) (Xu et al., 2019). Black carbon concentrations were measured by an aethalometer (AE33, Magee Scientific Corporation) (Zhao et al., 2017). Gaseous species, i.e., carbon monoxide (CO), sulfur dioxide (SO_2), ozone (O_3), nitrogen dioxide (NO_2), and nitric oxide (NO), were collected by Thermo Scientific gas analysers (Xu et al., 2019). CCN number concentrations were measured by a Droplet Measurement Technologies cloud condensation nuclei counter (DMT-CCNc) (Lance et al., 2006).

2.2. Source apportionment analysis

The PMF model is an extensively used multivariate factor receptor model for source apportionment (Paatero, 1999). In this study, size-resolved particle number concentrations (PNSD) measured by the SMPS and Gf-PDFs measured by the HTDMA system were input to the PMF model (US EPA PMF 5.0) to investigate the influence of various potential sources on their hygroscopic properties. The uncertainty is determined by the limit of detection and the relative uncertainty of each variable. Here a typical uncertainty calculated method was used in the PMF model for each species as Ogulei et al. (2006):

$$S_{ij} = \delta_{ij} + C \times X_{ij} \tag{1}$$

$$\delta_{ij} = \alpha \times \left(X_{ij} + \overline{X}_j \right) \tag{2}$$

where X_{ij} is the measured concentration for size bin j of the ith sample. C is a constant value and can be determined by a trial-and-error method from 0.01 to 0.5. The error term δ_{ij} is the estimated measurement error for the size bin j of the ith sample. α is a constant assumed commonly to be 0.01 for all size bins, and $\overline{X}_j$ is the measured mean concentration for size bin j. Since the PMF factor profiles were mainly driven by PNSD data, the uncertainty of the hygroscopic growth factor from each size bin was down-weighted by a factor of two (Vu et al., 2021; Beddows and Harrison, 2019).

In the PMF analysis, size-resolved particle number concentrations and growth factors were averaged to an hour resolution to reduce the

uncertainty caused by time lags between the SMPS and HTDMA systems. From the size PMF analysis, 30 random runs for 2 to 8 factors were evaluated with the variation in the Q value and the error estimation for selecting the optimal factor number. Solution selections with the number of factors were based on both the error analysis and physical interpretability of factors in terms of diurnal patterns and the correlation between external variables and factor profiles. Choosing the optimal number of factors is difficult due to the uncertainty of PMF analysis, including the random errors and rotational ambiguity (Paatero et al., 2014). The error estimations were examined via the bootstrap (BS) and displacement (DISP) in PMF analysis. After the additional diagnostics analysis, the appropriate number of factors has been chosen. Fpeak was to further found the minimum and stable Q. By comparing the base run with the selected Fpeak run, the uncertainty of the results is ±22%. After a careful evaluation of the output from PMF model, six factors were finally selected as the best solutions for the datasets from winter 2016, and five were resolved for the PNSD datasets from winter 2014. Details about the diagnostics of PMF results appear in the Supplementary Information.

In addition, the source apportionment of organic aerosol (OA) obtained from HR-AMS was also analysed by using PMF (Xu et al., 2019) in two campaigns. In winter of 2014, five OA factors was selected, including three primary organic aerosols (POA) factors namely, cooking OA (COA), coal combustion OA (CCOA) and biomass burning OA (BBOA), and two secondary organic aerosols (POA) factors from less-volatile oxygenated OA (LV-OOA) and semi-volatile oxygenated OA (SV-OOA). For the winter of 2016, six-factor solution was chosen, including three POA factors namely COA, BBOA and fossil fuel-related OA (FFOA), and three SOA factors from oxidized POA (OPOA), oxygenated OA (OOA), and aqueous-phase OOA (aq-OOA). Detailed operations about the HR-AMS and PMF solutions can be found in Xu et al. (2019).

2.3. Calculation of CCN number concentration

In this study, the N_{CCN} calculation was based on κ-Köhler theory using PNSD and the critical diameter (D_{cut}) (Ren et al., 2018; Zhang et al., 2019). PNSDs and mean Gfs of different factors can be obtained from the PMF analysis.

As proposed by Petters and Kreidenweis (2007), the method to derive D_{cut} is based on κ-Köhler theory, with the water vapor saturation ratio over the aqueous solution droplet S given by:

$$S = \frac{D^3 - D_P^3}{D^3 - D_P^3(1-\kappa)} exp\left(\frac{4\sigma_w M_w}{RT\rho_w D}\right) \tag{3}$$

$$\kappa = \frac{4\left(\frac{\sigma_w M_w}{RT\rho_w}\right)^3}{27 D_p^3 \, ln^2 S_c} \tag{4}$$

$$D_{cut} = \sqrt[3]{\frac{4\left(\frac{\sigma_w M_w}{RT\rho_w}\right)^3}{27\kappa \, ln^2 S_c}} \tag{5}$$

where D is the droplet diameter, D_p is the dry diameter of the particle, M_w is the molecular weight of water, σ_w is the surface tension of pure water, ρ_w is the density of water, R is the gas constant, and T is the absolute temperature. D_p is also the critical diameter for the given S when κ is known.

The hygroscopicity parameter for different factors can be derived from the Gf according to the κ-Köhler theory (Petters and Kreidenweis, 2007):

$$\kappa_{gf_i} = \left(Gf_i^3 - 1\right) \bullet \left[\frac{1}{RH} exp\left(\frac{4\sigma_{s/a} M_w}{RT\rho_w D_d Gf_i}\right) - 1\right] \tag{6}$$

where Gf_i is the Gf for factor i, RH is the relative humidity in the HTDMA

(90% used in this study), D_d is the dry diameter, $\sigma_{s/a}$ is assumed to be the surface tension of pure water, R is the universal gas constant, T is the temperature, M_w is the molecular mass, and ρ_w is the density of water.

Then N_{CCN} for a given factor can be calculated as

$$CCN_{pre-i} = \int_{D_{cut-i}}^{D_{end}} n\left(log\, D_{p-i}\right) d\, log\, D_{p-i} \tag{7}$$

For the factor i, where D_{cut-i} is the upper-limit diameter of the PNSD for factor i, and D_{end} is the lower-limit diameter, $n_{(log\, Dp-i)}$ is a function of the aerosol number size distribution. The total N_{CCN} is the sum of N_{CCN} for different factors.

3. Results

3.1. Resolved PNSD and Gf-PDF by the PMF model

Fig. 1 shows the time series of field observed data in urban Beijing during winter of 2016, including the PNSD, Gf-PDFs, particle mass concentrations, meteorological parameters, and gaseous species concentrations. By combining the field observations and a positive matrix factorization model, we identified hygroscopic properties of aerosol particles from six different sources that are indicated by six factors as shown in Fig. 2. Factor 1 was dominated by nucleation-mode particles peaking at around 20 nm, associated with a new particle formation (NPF) event from photochemistry (Dai et al., 2021). The time series of N_{CN} show sharp peaks mostly on clean days (Fig. 2a). Diurnal variations of N_{CN} also show peaks during NPF events (09:00–14:00 local time, LT) (Fig. 3a$_2$). The corresponding Gf-PDF for the nucleation mode was dominated by a hygroscopic mode with a Gf of ~1.3 when the NPF event occurred. A small hydrophobic mode is also seen, probably due to the influences of primary traffic emissions and the less-hygroscopic organics (Org) in newly formed particles (Zhang et al., 2004). The hygroscopic mode became more dominant around noon and the early afternoon. This suggests that the photochemical reaction promotes the particles growth through condensation and the aging process (Liu et al., 2021), and the transition of mixing state from externally mixed to internally mixed after NPF events occur (Wu et al., 2016). The enhancement of water-soluble compounds through photochemical process would lead to an increase in the hydrophilic mode (Chen et al., 2022). Note that there may be some uncertainties in this analysis because the HTDMA did not measure diameters below 40 nm, so not all features of newly formed particles were captured.

The size distribution of factor 2 shows a peak mode at 30–40 nm, mainly corresponding to traffic emissions consisting of particles with diameters ranging from 10 to 120 nm, as suggested previously (Vu et al., 2015; Pey et al., 2009). The time series of N_{CN} and Gf-PDF show large fluctuations during the observation period (Fig. 2b). The diurnal variation of N_{CN} (Fig. 3b$_2$) shows two pronounced peaks associated with traffic emissions during the morning and evening rush hours (eg., 8:00–9:00 LT and 19:00–20:00 LT). The correlation coefficient indicates high value with the vehicle exhaust NO$_x$ (Fig. 4). The PMF-derived Gf-PDF for traffic-related particles was dominated by a hydrophobic or less hygroscopic mode, with Gf less than ~1.2 (Fig. 3b$_3$), generally consistent with previous studies (Li et al., 2021; Vu et al., 2021). These particles mostly consisted of externally mixed hydrophobic particles from primary emissions (Wang et al., 2017). Two peaks of the hydrophobic/less hygroscopic mode during traffic hours were also indicated in the diurnal variation of GF-PDF (Fig. 3b$_4$).

Factor 3, associated with cooking emissions, shows two pronounced peaks in N_{CN} at lunch and dinnertime (eg., 12:00–13:00 LT and 19:00–20:00 LT) (Fig. 3c$_2$). The similar diurnal pattern was also observed for cooking organic aerosols (COA) (Du et al., 2017). In addition, the mean PNSD of factor 3 (Fig. 3b$_1$) shows characteristics of cooking sources, namely, a peak at ~50 nm (Harrison et al., 2011; Cai
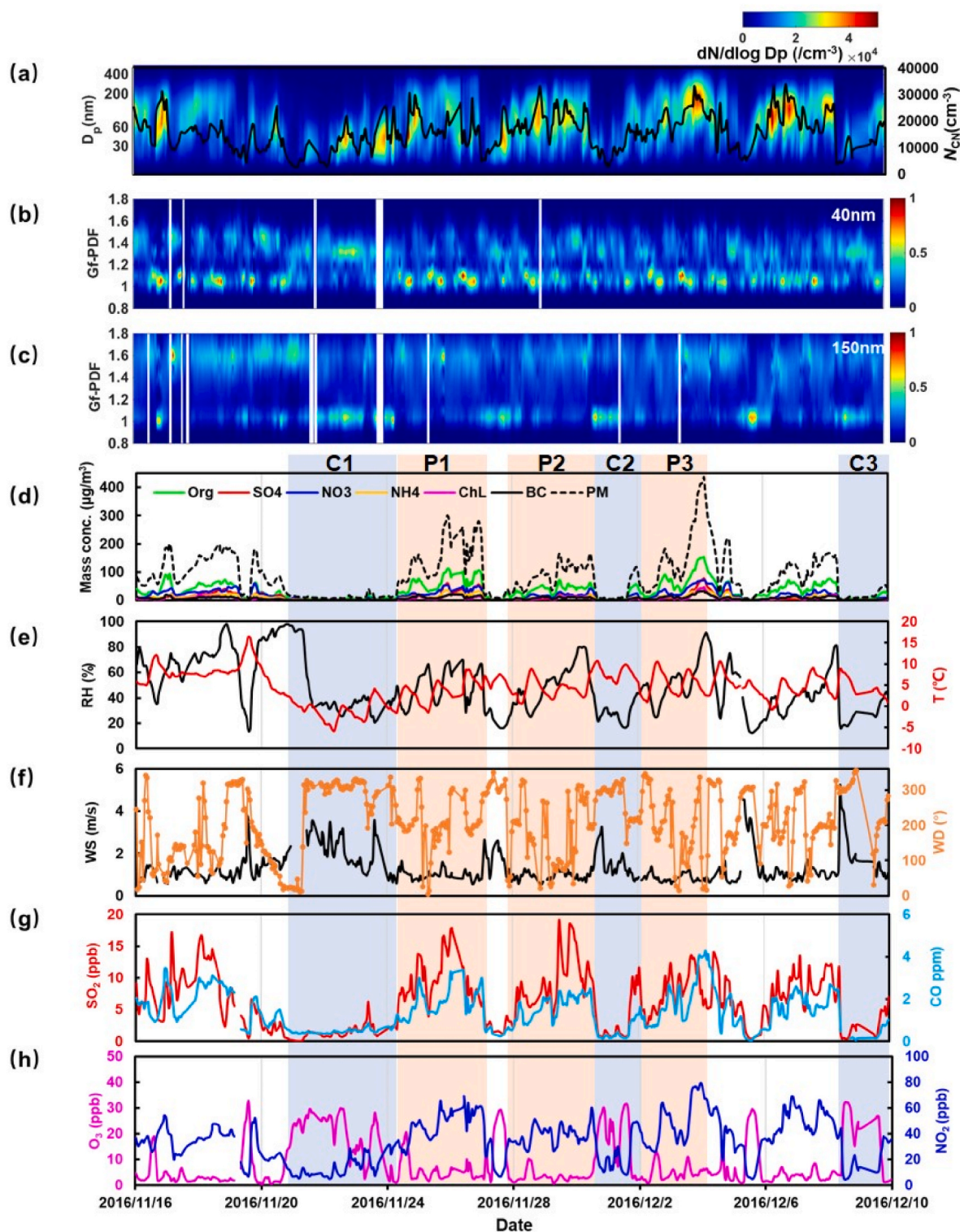
Fig. 1. Time series of (a) particle number size distribution (colored background) and particle number concentration (N_{CN}, black line), (b–c) growth factor probability distribution functions (Gf-PDFs) for 40 and 150 nm at relative humidity, RH = 90%, (d) PM_1 concentration, (e) RH and ambient temperature (T), (f) wind speed at 8 m and wind direction at 280 m above ground level, (g) SO_2 and CO concentrations, and (h) O_3 and NO_2 concentrations. Three clean cases (C1, C2, and C3) and three polluted cases (P1, P2, and P3) were selected for further investigation.

et al., 2020). Furthermore, N_{CN} correlates well with COA (Fig. 4). As with traffic emissions, the Gf-PDF for particles from cooking has a dominant mode of ~1.0 (Fig. 3c₃). The Gf-PDF thus showed hydrophobic modes during lunch and dinnertime (Fig. 3c₂ and 3c₄). At 18:00 LT, the fraction of hydrophobic-mode particles increased significantly, which may be due to increased cooking activities from nearby food stalls

at night (Zhao et al., 2017).

The mean PNSD for factor 4 was unimodal, with one peak around 100 nm. The correlation analysis suggests that this factor is not only associated with primary emissions but also well correlated with O_3 (Fig. 4; Du et al., 2021). N_{CN} was also characterized by higher values during nighttime and a small peak around noon (Fig. 3d₂). Similarly, the
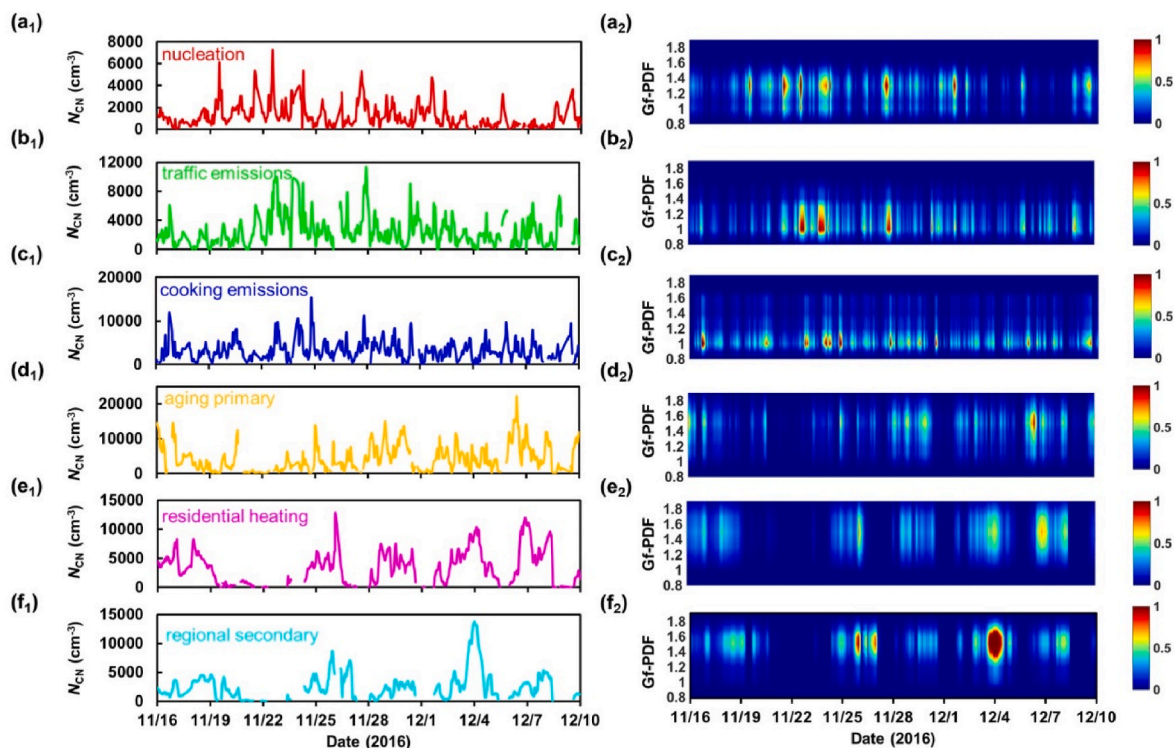
Fig. 2. PMF-derived time series of CN number concentrations (N_{CN}, left panels) and hygroscopic growth factor probability density functions (Gf-PDF, right panels) of different factors (from 16 November to 10 December of 2016). (a_1-a_2) Factor 1, nucleation sources; (b_1-b_2) factor 2, traffic emissions; (c_1-c_2) factor 3, cooking emissions; (d_1-d_2) factor 4, aging primary; (e_1-e_2) factor 5, residential heating; and (f_1-f_2) factor 6, regional secondary sources.

diurnal variation shows a conversion trend from primary organic aerosols (POA) to oxidized POA (Fig. S5), further suggesting that factor 4 represents the aging process. Thus, factor 4 is defined as the aging-primary-related source. The Gf-PDF for these particles is dominated by a hygroscopic mode with Gf of ~1.5 (Fig. 3d₃). A small hydrophobic mode was attributed to the disturbance of local primary emissions. The fraction of hygroscopic-mode particles greatly increased during nighttime. This is likely because heterogeneous and/or aqueous reactions promoted the aging process and growth of these primary particles at night (Fan et al., 2020). Particles from primary emissions could be internally mixed with the large particles by coagulation and thus grow rapidly, resulting in accumulated-mode particles with high hygroscopicity.

Factor 5 was dominated by the accumulation mode, peaking at around 150 nm (Fig. 3e₁). It is associated with gaseous tracers (e.g., SO_2, NO_x, and CO), correlating well with combustion-generated aerosols (Dai et al., 2021) (Fig. 4). Therefore, factor 5 is resolved as residential heating emissions. The diurnal pattern of N_{CN} for factor 5, with lower values during daytime and higher values at night, further illustrates this (Fig. 3e₂). The GF-PDF for particles from residential heating showed a strong hygroscopic mode of 1.4–1.6 reflecting the dominant sulfate particles from residential coal combustion in northern China (Dai et al., 2019). During late afternoon and nighttime, the hygroscopic mode became more dominant (Fig. 3e₄). This is likely because higher ambient RH at night may promote the production of sulfate through aqueous chemical reaction (Wang et al., 2015).

The mean PNSD for factor 6 had a peak at around 250 nm (Fig. 3f₁) and was highly correlated with the mass concentrations of secondary inorganic aerosols (SIA, including sulfate, nitrate, and ammonia) and secondary organic aerosols (SOA) (Fig. 4). Factor 6 was thus identified as a regional secondary source (Cai et al., 2020). It is characterized by a diurnal pattern of N_{CN} with high values during nighttime (Liu et al., 2016) (Fig. 3f). As expected, the hygroscopic growth factors of particles from the resolved regional secondary source were very hygroscopic,

with a Gf value of ~1.6. Similar, the peak mode of hygroscopic played the dominant role during nighttime mainly caused by the aqueous oxidation and the increment of aerosol liquid water to promote the formation and growth of sulfate, nitrate, and SOA (Wang et al., 2016; Wu et al., 2018). The coagulation process with larger particles also promoted particles quickly internally mixed and aged, thus enhanced the fraction of hygroscopic mode.

3.2. Numbers and mass fractions of the six PMF-resolved factors

Fig. 5 shows the average numbers and mass fractions of the six resolved PMF factors during the field campaign. The mass fraction was calculated by assuming that particles were spherical with a density of 1.5 g cm^{-3} (Hu et al., 2012), a value typically reported for urban cities in China. Note that the number concentration of cooking sources here was converted to mass concentration by assuming a density close to POA (~1.0 g cm^{-3}) (Wu et al., 2016). Diurnal variations show that both the numbers and mass fractions of nucleation, traffic-related, and cooking-related emissions increased considerably during daytime. The fractions of regional secondary and aging primary related sources largely increased during nighttime. On average, nucleation, traffic emissions, cooking emissions, aging primary, residential heating, and regional secondary sources contributed 7%, 15%, 20%, 26%,18%, and 14%, respectively, to the total particle number concentration. The aging primary source accounted for the largest number fraction during the observed period. Comparatively, its contribution to the mass concentration was much less, accounting for only 9% of the total particle mass concentration. Aerosol particles from regional secondary sources and residential heating dominated, contributing 82% to the total mass concentration although they only accounted for a relatively smaller portion of the number fraction. Traffic-related particles and cooking emissions are considered the major source of particles in the urban atmosphere (Du et al., 2017). In this study, traffic and cooking activities contributed significantly (~35%) to the total particle number concentration, but

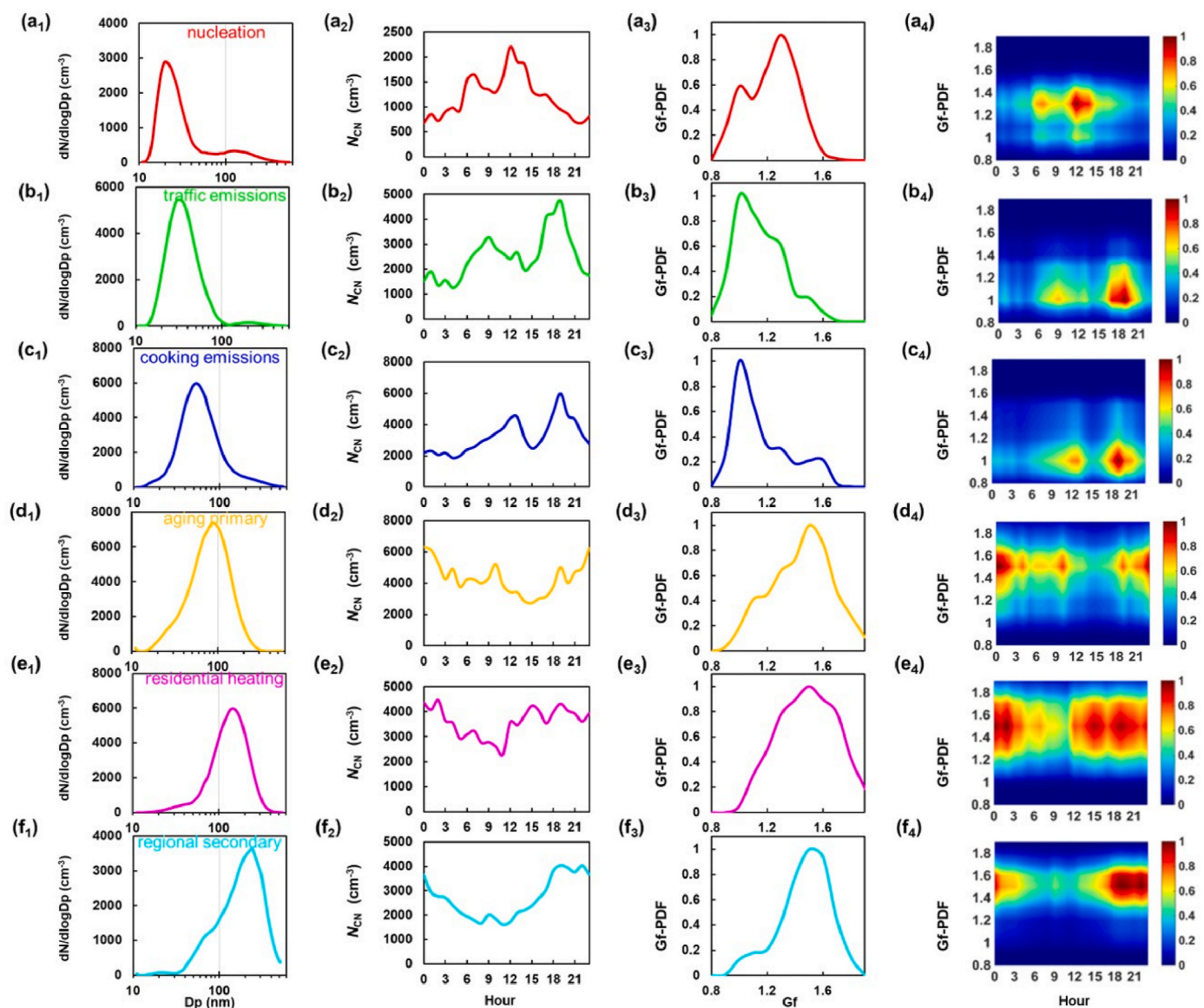**Fig. 3.** Mean particle number size (a_1, b_1, c_1, d_1, e_1, f_1) and Gf-PDF (a_3, b_3, c_3, d_3, e_3, f_3) distributions, and diurnal cycles of CN number concentration (a_2, b_2, c_2, d_2, e_2, f_2) and Gf-PDF (a_4, b_4, c_4, d_4, e_4, f_4) of the six PMF factors.

comparatively, they contributed a much smaller fraction (~7%) to the total mass concentration (Fig. 5c and d). The number fraction of cooking sources in this study was higher than that reported in an urban site (~7%) in London (Harrison et al., 2011). Nucleation-mode particles contributed the least to both the total number and mass concentrations during the observed period. Our results highlight the importance of reducing secondary aerosol particles to improve the regional air quality in the North China Plain.

3.3. Comparison of identified Gfs with those reported in the literature

The derived Gfs and hygroscopic parameter κ of the six PMF-resolved factors were compared with those reported in previous studies (Fig. 6 and Table 1). Here, results measured from field campaigns (Vu et al., 2021; Sakurai et al., 2005; Wu et al., 2017) and laboratory studies (Tritscher et al., 2011; Li et al., 2018) were reviewed. To ensure the comparability of results among different studies, only Gf values measured at RH = 90% or close to 90% were selected.

For particles from nucleation, the mean Gf value assigned by the PMF analysis in this study was 1.23 ± 0.05 (corresponding to a κ value of 0.15

$\pm$ 0.03), within the range of 1.1–1.6 reported in the literature. The value derived in this study is more comparable with that reported by Hämeri et al., (2001) and Vu et al. (2021) who also used the HTDMA system to obtain results. However, higher Gf values of ~1.4–1.6 for newly formed particles were observed in urban sites in Atlanta (Sakurai et al., 2005), Gosan (Buzorius et al., 2004), and Marseilles (Petäjä et al., 2007), likely because newly formed particles in these areas are dominated by the oxidation of SO_2 (McMurry et al., 2005; Petäjä et al., 2007; Kim et al., 2011). The hygroscopic properties of nucleation-mode particles could be closely related to the properties of condensing vapors as well as the growth mechanism, leading to diverse hygroscopic properties across different regions.

The mean Gf value for particles from traffic sources is 1.15 ± 0.02, within the range of 1.0–1.29 reported in previous studies. Our derived Gf value is slightly higher than those reported from chamber experiments (Tritscher et al., 2011) but comparable with results measured in the ambient atmosphere (Vu et al., 2021). This is likely because particles may be converted from nearly hydrophobic to hygroscopic during the atmospheric aging process. Generally, aerosol particles from
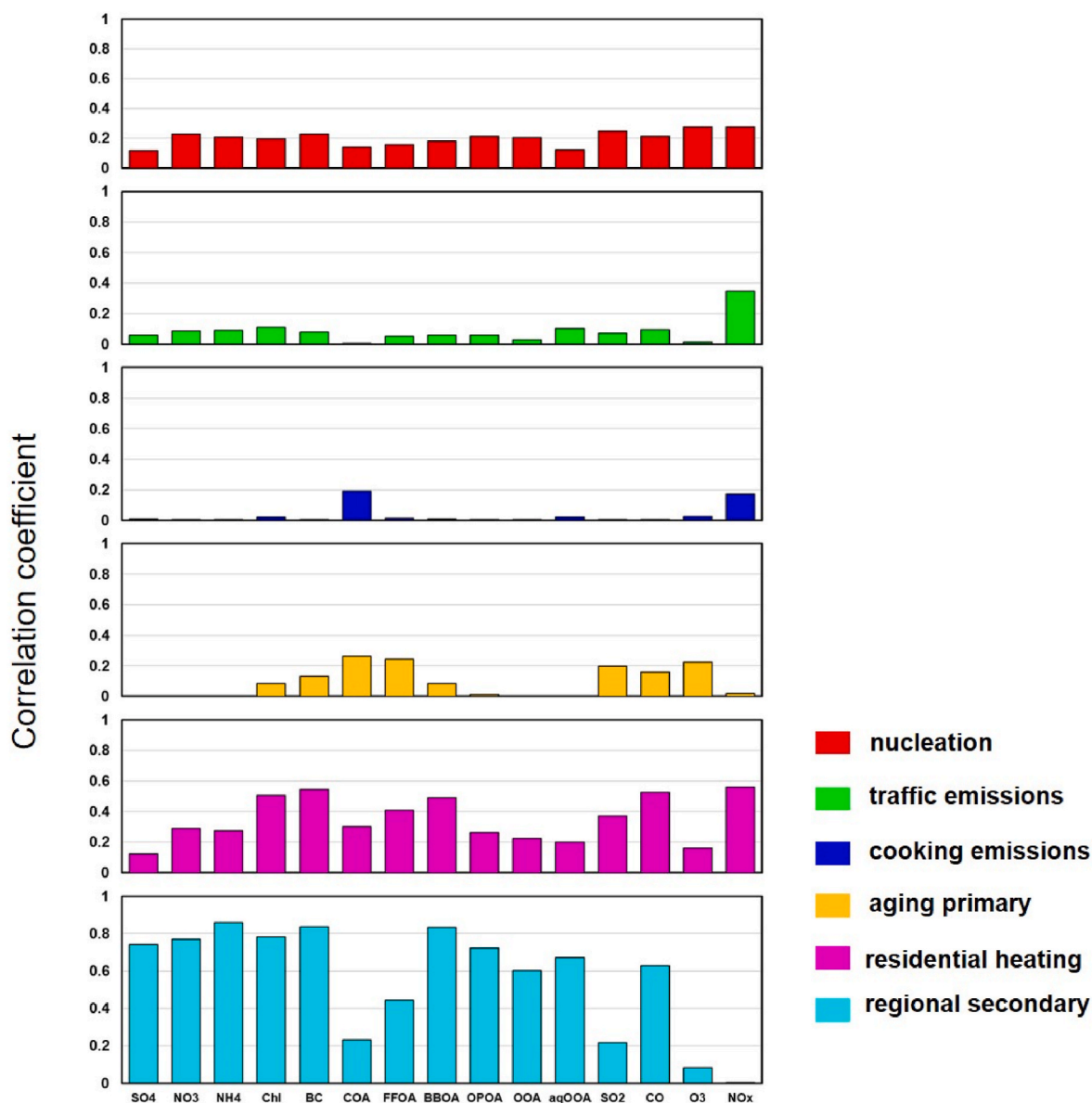
Fig. 4. The correlation coefficients between PMF factors and tracer pollutants including, SO_4, NO_3, NH_4, Chl, BC and SO_2, CO, O_3, NO_x. Organics are produced from COA, FFOA, BBOA, OPOA, OOA, aq-OOA in the winter of 2016.

traffic-related emissions are less hygroscopic in most cases, with a mean κ value of <0.13.

Particles from cooking activities were considered to be a mixture of fresh and aged COA, with a mean Gf value of 1.17 ± 0.11, ranging from 1.08 to 1.25. Previous studies have shown that freshly emitted COA would become more oxygenated by reacting with O_3 and OH radicals, thus increasing the potential capacity of CCN activity (Li et al., 2018; Kaltsonoudis et al., 2017). The derived Gf values in this study correspond to a mean κ of 0.10 ± 0.07, which falls in the range of values reported from chamber experiments for fresh and aged cooking particles (Li et al., 2018).

Particles related to the aging primary process are more hygroscopic, with a mean Gf value of 1.44 ± 0.04. These particles are considered to be mixtures of primary emissions from combustion and aged accumulation-mode particles. Recent studies have indicated that 40–80% of fossil fuel-primary organics aerosols in urban Beijing were water soluble (Qiu et al., 2019). Particles from residential heating also show a more hygroscopic mode with a Gf value of 1.48 ± 0.03, similar to particles emitted from district heating plants (Rissler et al., 2005). The

hygroscopic properties of secondary aerosol particles, which originate from regional transport and secondary formation (Cai et al., 2020), are similar to those from residential heating. The dominance of more hygroscopic compounds (e.g., SIA and SOA) in the accumulation mode explains the high Gf value. For example, Vu et al. (2021) reported Gf values of ~1.34–1.48 for mixed SOA and SIA, comparable to our results.

Overall, the hygroscopic properties of aerosol particles vary with variabilities in emission sources, environmental conditions, and atmospheric processing (Swietlicki et al., 2008 and references therein). The variability in aerosol particle hygroscopicity depends highly on the composition, as shown in Fig. S6. Overall, the more hygroscopic particles in many cases were from residential heating and regional transportation during the field campaign.

3.4. Case study: attributing Gfs on clean and polluted days using the PMF-resolved factors

To illustrate the impacts of various sources on the hygroscopic properties of particles under different pollution conditions, six cases
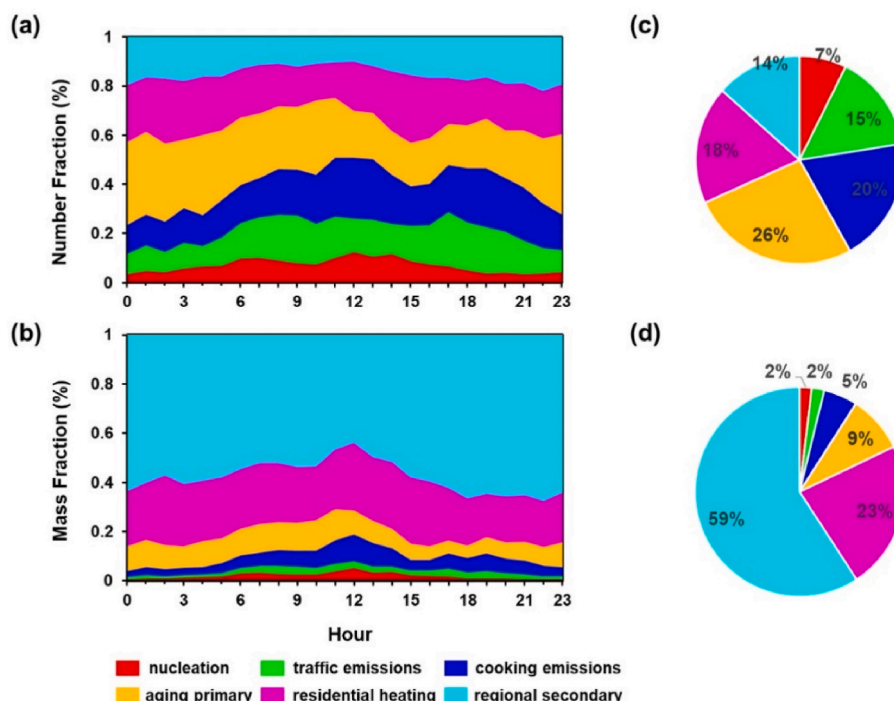
Fig. 5. Average diurnal variations of number (a) and mass fraction (b) of the six PMF-derived factors during the observed period. Pie charts show the campaign (c) average number and (d) mass fraction of the different factors.
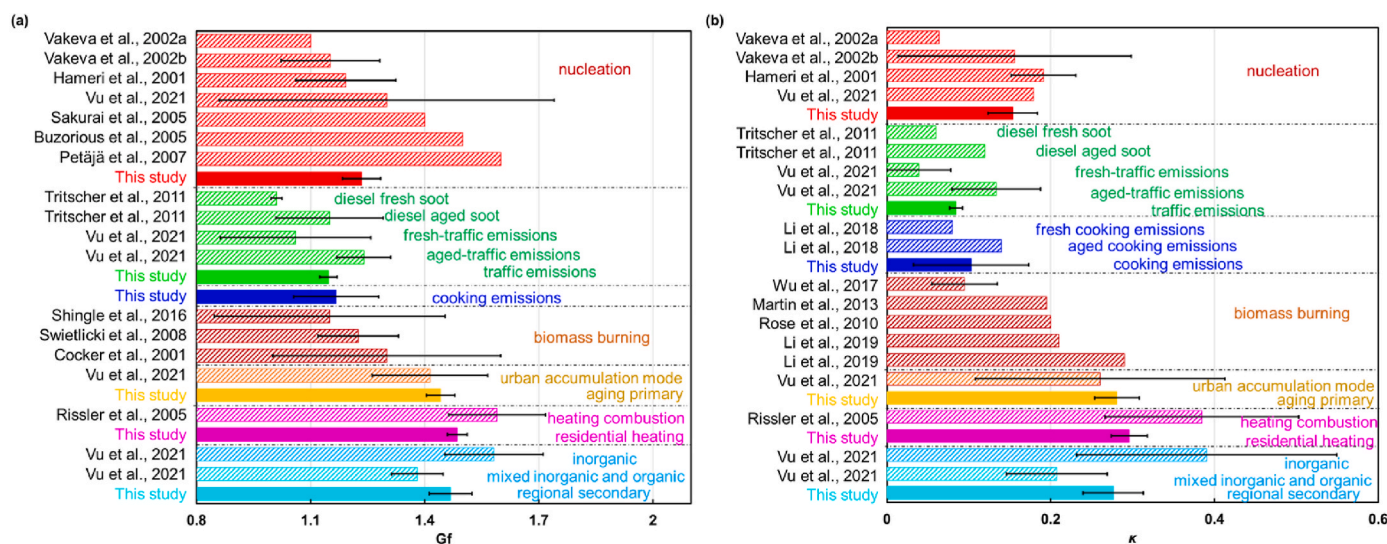

Fig. 6. Comparisons of PMF-resolved hygroscopic properties with the reported literatures (a) Gf and (b) hygroscopic parameter (κ) from this study and from the literatures.

representing polluted and clean conditions were chosen for further investigation (Fig. 7). Gf values of particles under polluted conditions were larger than those under clean conditions except for 40-nm particles. This can be explained by differences in the number concentration or fraction of the resolved PMF factors between polluted and clean cases. Fig. 7 shows that under polluted (clean) conditions, hygroscopic sources represented by aged and secondary processes contributed 55–78% (20%) to the N_{CN}. For 40-nm particles, Gf values were larger on clean days when photochemical-nucleation-sourced particles dominated the population of small particles. Under polluted conditions, small particles were mainly from local primary sources, e.g., traffic and cooking (Fan et al., 2020), leading to lower Gf values. The contribution from

nucleation sources increased from 2–6% under polluted conditions to 17–26% during clean periods. This suggests that the source apportionment of Gfs can well interpret the variation in hygroscopic properties under different atmospheric pollution conditions.

3.5. Using PMF-resolved Gfs to predict N_{CCN}

Extrapolations of HTDMA data to water vapor supersaturation have been shown to accurately predict the CCN activity of aerosols (Cai et al., 2018). Here, we attempt to estimate N_{CCN} using PMF-resolved Gfs and PNSDs from different sources, drawing conclusions regarding characteristic CCN properties among various sources. The activation, or critical

Table 1

Summary of hygroscopic growth factor (Gf) values and hygroscopic parameters (κ) from different sources reported in the literature and PMF-modeled results from this study.

Sources	Diameter	RH	Gf	κ	References
nucleation	8–10 nm	90%	~1.1	0.06	Väkevä et al. (2002a)
nucleation	20 nm	90%	1.15 ± 0.13	0.16 ± 0.14	Väkevä et al. (2002b)
nucleation	10–20 nm	90%	1.19 ± 0.13	0.19 ± 0.04	Hämeri et al. (2001)
nucleation	50 nm	90%	1.30 ± 0.44	0.18	Vu et al. (2021)
nucleation	10 nm	90%	~1.4		Sakurai et al. (2005)
nucleation	25 nm	83%	1.5		Buzorius et al. (2004)
NPF day	20–50 nm	88%	~1.6		Petäjä et al. (2007)
nucleation	40 nm	90%	1.23 ± 0.05	0.15 ± 0.03	**this study**
traffic	35–300 nm	95%	1–1.02		Tritscher et al. (2011)
traffic	50–100 nm	95%	1.05–1.25	0.06–0.12	Tritscher et al. (2011)
traffic-fresh	50, 75 nm	90%	0.92–1.20	0.04 ± 0.03	Vu et al. (2021)
traffic-aged	50, 75 nm	90%	1.19–1.29	0.13 ± 0.05	Vu et al. (2021)
traffic	40, 110 nm	90%	1.15 ± 0.02	0.08 ± 0.01	**this study**
cooking-fresh				0.08	Li et al. (2018)
cooking-aged				0.14	Li et al. (2018)
cooking	40, 80 nm	90%	1.17 ± 0.11	0.10 ± 0.07	**this study**
Biomass Burning		85%		0.2	Rose et al. (2010)
BB	50, 150 nm	89%	1.3 ± 0.30		Cocker et al. (2001)
BB			1.23 ± 0.11		Swietlicki et al. (2008)
BB	175, 350 nm	83%	1.15 ± 0.30		Shingler et al. (2016)
BB				0.195	Martin et al. (2013)
BB event	50–250 nm			0.09–0.10	Wu et al. (2017)
BB (fresh)				0.21	Li et al. (2019)
BB (aged)				0.29	Li et al. (2019)
Urban accumulation mode (acc.)	acc.	90%	1.41 ± 0.15	0.26 ± 0.15	Vu et al. (2021)
aging primary	80, 110 nm	90%	1.44 ± 0.04	0.28 ± 0.03	**this study**
heating	105 nm	90%	1.59 ± 0.13	0.38 ± 0.12	Rissler et al. (2005)
heating	150, 200 nm	90%	1.48 ± 0.03	0.30 ± 0.02	**this study**
inorganic	acc.	90%	1.58 ± 0.13	0.39 ± 0.16	Vu et al. (2021)
mixed	acc.	90%	1.38 ± 0.07	0.21 ± 0.06	Vu et al. (2021)
regional secondary	150, 200 nm	90%	1.47 ± 0.06	0.28 ± 0.04	**this study**

diameter of each individual source was calculated from its corresponding hygroscopic parameter at a given supersaturation using Köhler theory (Petters and Kreidenweis, 2007) (Fig. 8). The critical diameter of pure ammonia sulfate is also presented for comparison purposes. Retrieved critical diameters are, in general, larger than that expected for pure ammonia sulfate, indicating that even particles from those more hygroscopic sources may consist of both organic and inorganic material.

The calculated critical diameters, along with PNSDs in the winter of 2016 were used to evaluated the performance of predicting N_{CCN} by using the resolved Gf from various sources. Here, we examined PNSDs observed in urban Beijing in the winter of 2014. First, the PMF model was used to resolve particle source factors based on these PNSDs. Five factors, i.e., traffic, cooking, aging primary particles, residential heating, and secondary related sources, were resolved (Fig. S7). The PMF source factors resolved for this dataset observed in 2014 were almost the same as those observed in 2016 because both campaigns were conducted at the same site and in the same season. Calculated critical diameters of different source factors (Fig. 8) were then applied to predict the N_{CCN} of corresponding PMF factors using the resolved PNSDs.

Fig. 9 shows comparisons of predicted and measured N_{CCN} at S = 0.23% during the 2014 field campaign. Overall, the time series of predicted and observed N_{CCN} agree well. The CCN number concentration was calculated with an acceptable overestimation of ~19% (coefficient of determination, $R^2 = 0.99$) at S = 0.23%. Further analysis shows that the overestimation between predicted and measured N_{CCN} became more pronounced at night (Fig. 9c, Fig. S8), likely due to the significant increase in Org mass loadings during the same periods in 2014 (Fig. S9). The hygroscopic properties and CCN activity of organic matter have large uncertainties due to its complex composition (Liu et al., 2021). Note that the method for predicting N_{CCN} has some limitations. Since aerosol particle chemical compositions vary with time and region, this will lead to uncertainties in Gf values or critical diameters even from the same PMF-sourced factor from different sites (see Fig. 6). Also, the PMF method itself has some uncertainties (Ogulei et al., 2006; Paatero et al., 2014). It is thus necessary to examine more observational data to verify this methodology. More importantly, developing a comprehensive dataset including more Gf and critical diameter results from more diverse sources based on field investigations is warranted so that estimates of N_{CCN} in different regions and different times of the year can be made.

3.6. Source apportionment of cloud nuclei

Fig. 10 shows the contributions of different resolved sources to N_{CN} and N_{CCN}. The total contribution of particles originating from the aging process and residential heating and regional secondary sources to N_{CCN} were greater than 90%. The contribution from these sources reached as high as 97% for polluted cases. This is expected because particles emitted from these sources were more hygroscopic, and their size distributions peaked in the accumulation mode (Figs. 3 and 6). Under polluted conditions, particles from residential heating contributed the most to N_{CCN} due to the formation of very hygroscopic sulfate from residential coal combustion (Dai et al., 2019; Li et al., 2017). On clean days, particles related to the aging process contributed the most to N_{CCN}, suggesting the critical role of photochemical processes in changing particle CCN activity. Although particles from primary emissions (traffic and cooking activities) contributed greatly to N_{CN} under both clean and polluted conditions, their contributions to N_{CCN} were only 17% on clean days and 3% on polluted days. On average, the total contribution from the two sources was 5%. This demonstrates the important roles of secondary and aging processes in elevating CCN levels in urban Beijing.

4. Conclusions

Aerosols hygroscopicity, which highly depends on the particle emission sources, plays critical role in evaluating their effects on cloud formation. It is thus critical to characterize the hygroscopic properties of aerosol particles from different sources. In this study, we performed source apportionment analysis by applying a PMF model to field measured PNSD and Gf-PDF datasets in urban Beijing to identify hygroscopic Gfs of fine aerosol particles from different sources. Six factors, i.e., the nucleation process, traffic emissions, cooking activities, aging primary, residential heating, and regional secondary, were resolved,
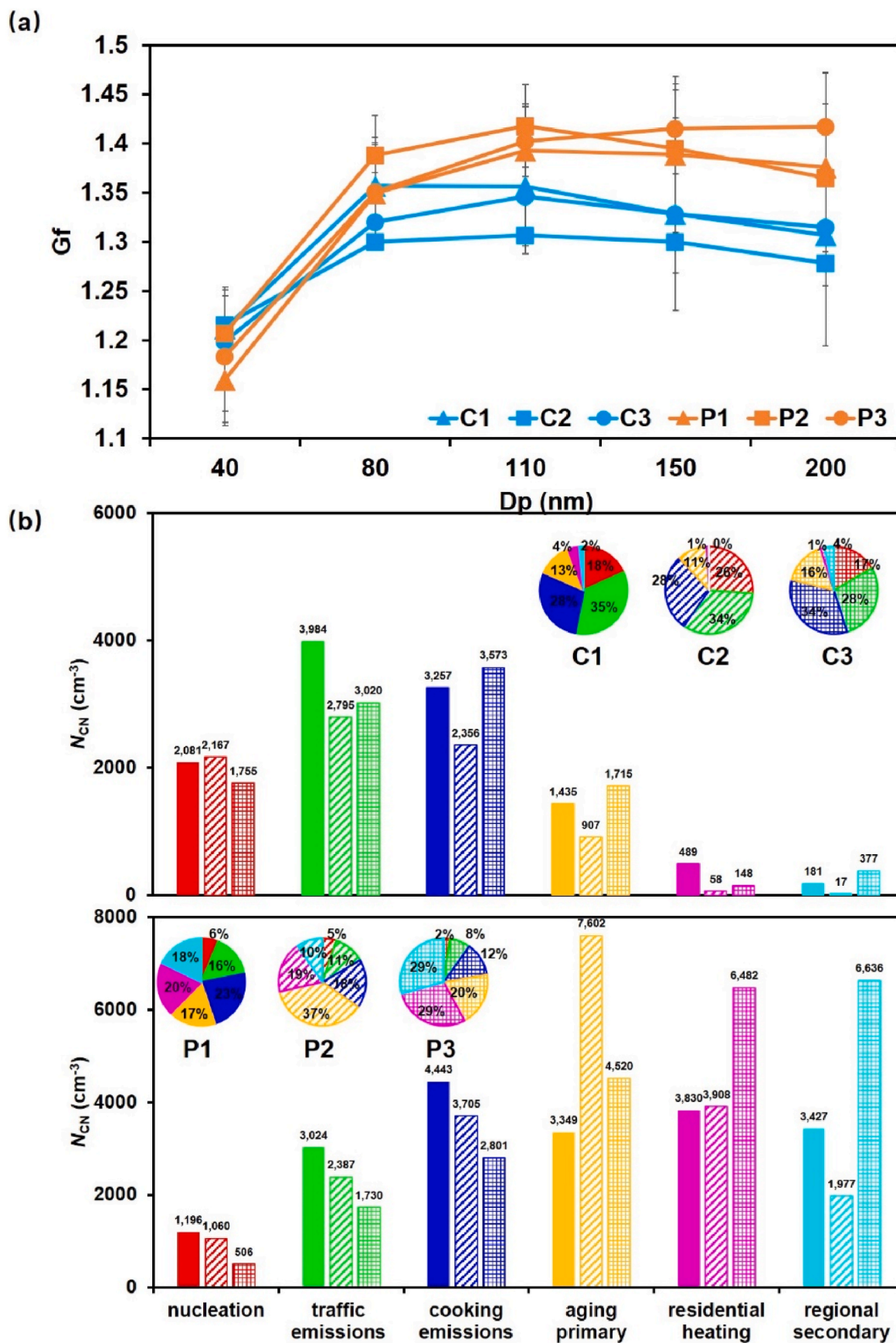
Fig. 7. Size-resolved mean growth factors (Gf) on D_p for clean (C1–3) and polluted (P1–3) cases (a), and the average number concentration (N_{CN}) of each factor (b). Measurements are from the winter of 2016.
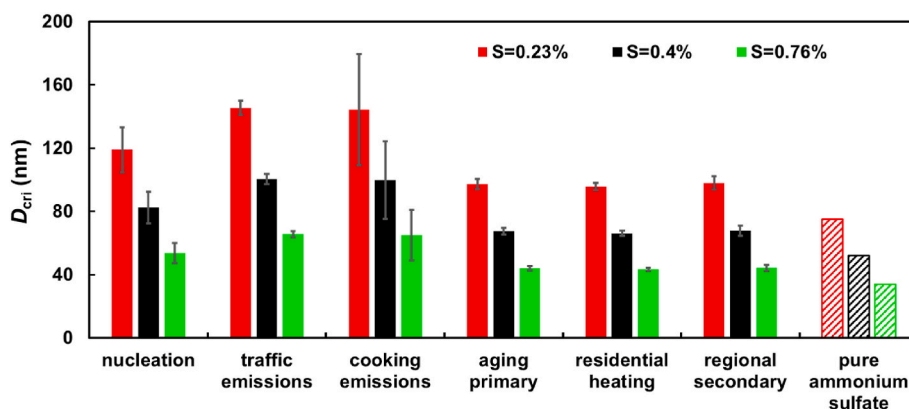
Fig. 8. Calculated critical diameters (D_{cri}) at S = 0.23%, 0.40%, and 0.76% for aerosol particles from different sources and for pure ammonium sulfate.
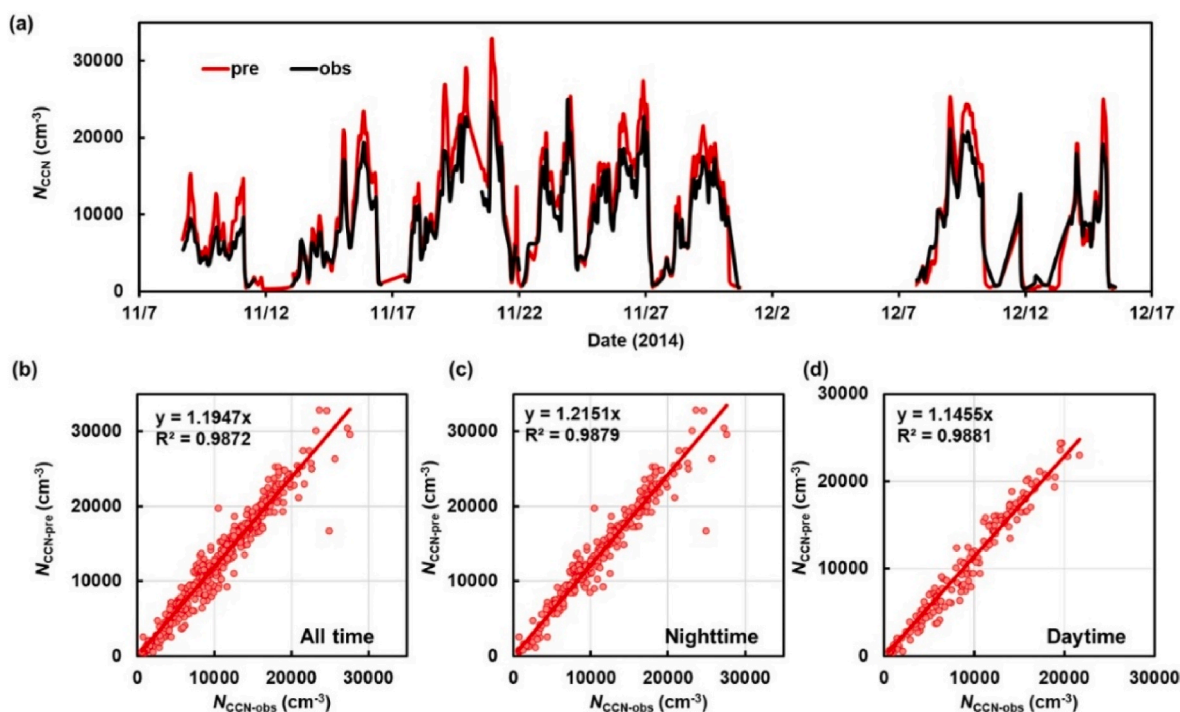

Fig. 9. Time series of the observed and predicted N_{CCN} at S = 0.23% in the winter of 2014 (a), scatter plots data from all time periods (b), nighttime only (17:00–06:00 LT) (c), and daytime only (06:00–17:00 LT) (d).

with mean Gf values of 1.23, 1.15, 1.17, 1.44, 1.48, and 1.47, respectively. These results are comparable to those reported in the literature. Furthermore, we applied the PMF-resolved Gfs to calculate the critical diameter among various sources based on the κ-Köhler theory. The N_{CCN} was then estimated within an acceptable overestimation of ~19% (R^2 = 0.99) at a typical supersaturation in cloud (S = 0.23%) using the critical diameters combined with PNSDs measured in another field campaign conducted in urban Beijing during the winter of 2014. Previous studies based on the bulk κ (eg., κ_{chem} derived from chemical composition) with PNSDs show that a significant overestimation of ~30%–50%, and even higher in some cases when estimating the CCN number concentration at S = 0.23% (Wang et al., 2010; Zhang et al., 2017). This indicates that the using Gfs among various sources in the calculation of CCN number concentration is worth promoting. The results show that the particles originating from secondary, aging, and residential-heating-related sources contributed greater than 90% of the total cloud nuclei. These results illustrate the critical roles of secondary and aging processes in elevating CCN levels in urban Beijing. The

contribution of particles from primary emissions (traffic and cooking activities) was ~5%, although they contributed greatly to total aerosol particle number concentrations. But these primarily emitted particles may experience aging and secondary conversion rapidly (Ren et al., 2018), and the mass fraction of soluble (Li et al., 2018) or the degree of oxidation (Kaltsonoudis et al., 2017) may enhanced greatly, serving as effective CCN.

The method used to predict N_{CCN} has limitations. Since aerosol particle compositions vary with time and region, this may lead to uncertainties in Gf values or critical diameters from the same PMF-sourced factor from different sites. Also, the PMF method itself has some uncertainties. It is thus necessary to examine more observational data to verify this methodology. Moreover, to predict CCN in different regions and different times of the year, developing a comprehensive dataset, including more Gfs or critical diameters from diverse sources based on field investigations, is warranted.
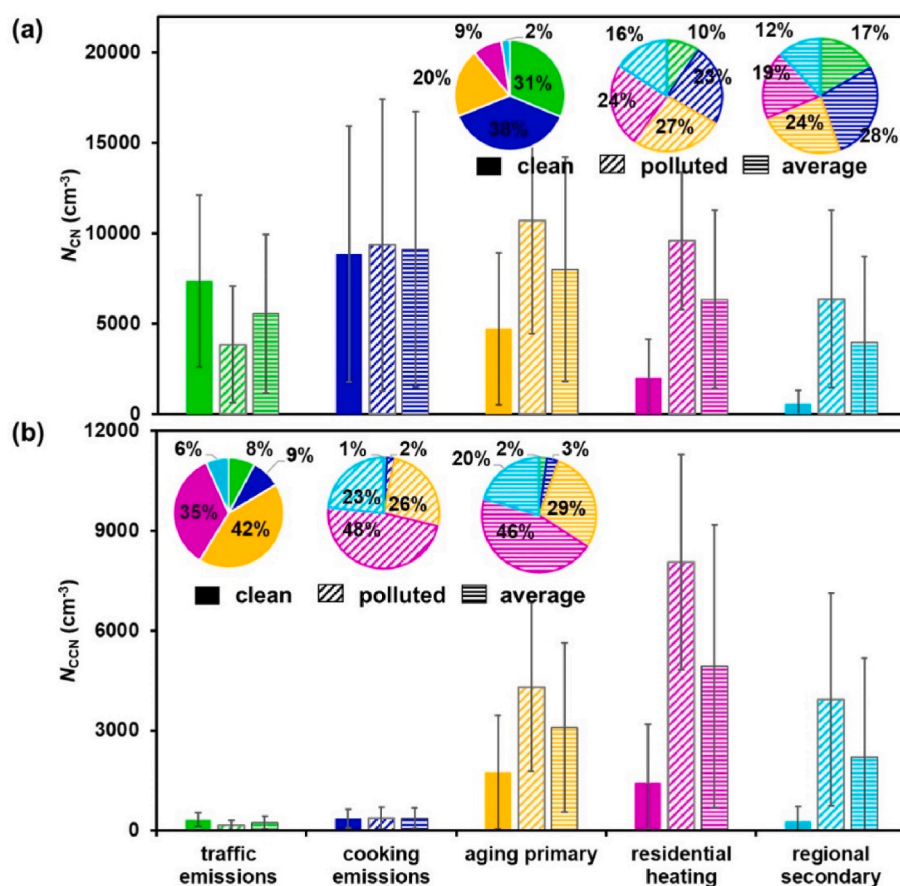
Fig. 10. Mean CN number concentration (N_{CN}) (a) and CCN number concentration (N_{CCN}) (b) from PMF-resolved sources under polluted and clean conditions during the field campaign of winter 2014 in urban Beijing. Here, "clean" represents cases where $PM_1 < 50 \mu g\ m^{-3}$, and "polluted" corresponds to cases where $PM_1 \geq 50 \mu g\ m^{-3}$ "Average" is the mean value during the field campaign.

CRediT authorship contribution statement

Jingye Ren: Conceptualization, Investigation, Formal analysis, Writing – original draft. **Fang Zhang:** Conceptualization, Supervision, Writing – review & editing, Funding acquisition. **Lu Chen:** Formal analysis. **Gang Cao:** Writing – review & editing. **Mengyu Liu:** Formal analysis. **Xue Li:** Data curation. **Hao Wu:** Technical support. **Yiling Cheng:** Formal analysis. **Zhanqing Li:** Writing – review & editing.

Declaration of competing interest

The authors declare that they have no known competing financial interests or personal relationships that could have appeared to influence the work reported in this paper.

Data availability

Data will be made available on request.

Acknowledgments

Appendix A. Supplementary data

Supplementary data to this article can be found online at https://doi.org/10.1016/j.atmosenv.2023.119615.

References

Bäumer, D., Vogel, B., et al., 2008. Relationship of visibility, aerosol optical thickness and aerosol size distribution in an ageing air mass over South-West Germany. Atmos. Environ. 42 (5), 989–998. https://doi.org/10.1016/j.atmosenv.2007.10.017.
Beddows, D.C.S., Harrison, R.M., 2019. Receptor modelling of both particle composition and size distribution from a background site in London, UK - a two-step approach. Atmos. Chem. Phys. 19, 4863–4876. https://doi.org/10.5194/acp-19-4863-2019.
Buzorius, G., et al., 2004. Secondary aerosol formation in continental outflow conditions during ACE-Asia. J. Geophys. Res. Atmos. 109 (D24) https://doi.org/10.1029/2004JD004749.
Cheng, Y.F., et al., 2008. Relative humidity dependence of aerosol optical properties and direct radiative forcing in the surface boundary layer at Xinken in Pearl River Delta of China: an observation based numerical study. Atmos. Environ. 42, 6373–6397. https://doi.org/10.1016/j.atmosenv.2008.04.009.
Cai, M., et al., 2018. The size-resolved cloud condensation nuclei (CCN) activity and its prediction based on aerosol hygroscopicity and composition in the Pearl Delta River (PRD) region during wintertime 2014. Atmos. Chem. Phys. 18 (16), 437. https://doi.org/10.5194/acp-18-16419-2018, 419–16.
Chen, L., et al., 2022. Measurement report: hygroscopic growth of ambient fine particles measured at five sites in China. Atmos. Chem. Phys. 22, 6773–6786. https://doi.org/10.5194/acp-22-6773-2022.
Cai, J., et al., 2020. Size segregated particle number and mass concentrations from different emission sources in urban Beijing. Atmos. Chem. Phys. 20, 12721–12740. https://doi.org/10.5194/acp-20-12721-2020.
Cocker, D.R., Whitlock, N.E., Flagan, R.C., Seinfeld, J.H., 2001. Hygroscopic properties of Pasadena, California aerosol. Aerosol Sci. Technol. 35, 637–647. https://doi.org/10.1080/027868201316899992.
Dai, Q., et al., 2021. Changes in source contributions to particle number concentrations after the COVID-19 outbreak: insights from a dispersion normalized PMF. Sci. Total Environ. 759 https://doi.org/10.1016/j.scitotenv.2020.143548.

Du, W., et al., 2017. Simultaneous measurements of particle number size distributions at ground level and 260 m on a meteorological tower in urban Beijing, China. Atmos. Chem. Phys. 17 (11), 6797–6811. https://doi.org/10.5194/acp-17-6797-2017.

Du, W., et al., 2021. Insights into vertical differences of particle number size distributions in winter in Beijing, China. Sci. Total Environ. 802 https://doi.org/10.1016/j.scitotenv.2021.149695.

Dai, Q., et al., 2019. Residential coal combustion as a source of primary sulfate in Xi'an, China. Atmos. Environ. 196, 66–76. https://doi.org/10.1016/j.atmosenv.2018.10.002.

Fan, X., et al., 2020. Contrasting size-resolved hygroscopicity of fine particles derived by HTDMA and HR-ToF-AMS measurements between summer and winter in Beijing: the impacts of aerosol aging and local emissions. Atmos. Chem. Phys. 20, 915–929. https://doi.org/10.5194/acp-20-915-2020.

Gysel, M., et al., 2009. Inversion of tandem differential mobility analyser (TDMA) measurements. J. Aerosol Sci. 40, 134–151. https://doi.org/10.1016/j.jaerosci.2008.07.013.

Happonen, M., et al., 2013. Diesel exhaust emissions and particle hygroscopicity with HVO fuel-oxygenate blend. Fuel 103, 380–386. https://doi.org/10.1016/j.fuel.2012.09.006.

Harrison, R.M., Beddows, D.C., Dall'Osto, M., 2011. PMF analysis of wide-range particle size spectra collected on a major highway. Environ. Sci. Technol. 45, 5522–5528. https://doi.org/10.1021/es2006622.

Hu, M., et al., 2012. Estimation of size-resolved ambient particle density based on the measurement of aerosol number, mass, and chemical size distributions in the winter in Beijing. Environ. Sci. Technol. 46 (18), 9941–9947. https://doi.org/10.1021/es204073t.

Hämeri, K., et al., 2001. Hygroscopic and CCN properties of aerosol particles in boreal forests. Tellus B 53 (4), 359–379. https://doi.org/10.1034/j.1600-0889.2001.530404.x.

Kandler, K., Schütz, L., 2007. Climatology of the average watersoluble volume fraction of atmospheric aerosol. Atmos. Res. 83, 77–92. https://doi.org/10.1016/j.atmosres.2006.03.004.

Kim, Y., et al., 2011. Characteristics of new particle formation and growth events observed at Gosan Climate Observatory in Fall 2009. Atmosphere 21, 35–44.

Kaltsonoudis, C., et al., 2017. Characterization of fresh and aged organic aerosol emissions from meat charbroiling. Atmos. Chem. Phys. 17, 7143–7155. https://doi.org/10.5194/acp-17-7143-2017.

Liu, J., et al., 2020. Increased aerosol extinction efficiency hinders visibility improvement in eastern China. Geophys. Res. Lett. 47 (20), e2020GL090167 https://doi.org/10.1029/2020gl090167.

Li, Y., et al., 2019. Cloud condensation nuclei activity and hygroscopicity of fresh and aged biomass burning particles. Pure Appl. Geophys. 176, 345–356. https://doi.org/10.1007/s00024-018-1903-0.

Lance, S., et al., 2006. Mapping the operation of the DMT continuous flow CCN counter. Aerosol Sci. Technol. 40, 242–254. https://doi.org/10.1080/02786820500543290.

Liu, J., et al., 2021. Hygroscopicity of organic aerosols linked to formation mechanisms. Geophys. Res. Lett. 48 https://doi.org/10.1029/2020GL091683.

Li, J., et al., 2021. Effects of chemical compositions in fine particles and their identified sources on hygroscopic growth factor during dry season in urban Guangzhou of South China. Sci. Total Environ. 801 https://doi.org/10.1016/j.scitotenv.2021.149749.

Liu, Z., et al., 2016. Source appointment of fine particle number and volume concentration during severe haze pollution in Beijing in January 2013. Environ. Sci. Pollut. Res. 23 (7), 6845–6860. https://doi.org/10.1007/s11356-015-5868-6.

Li, Y., et al., 2018. Cloud condensation nuclei activity and hygroscopicity of fresh and aged cooking organic aerosol. Atmos. Environ. 176, 103–109. https://doi.org/10.1016/j.atmosenv.2017.11.035.

Li, H., et al., 2017. Wintertime aerosol chemistry and haze evolution in an extremely polluted city of the North China Plain: significant contribution from coal and biomass combustion. Atmos. Chem. Phys. 17, 4751–4768. https://doi.org/10.5194/acp-17-4751-2017.

Massoli, P., et al., 2009. Aerosol optical and hygroscopic properties during TexAQS-GoMACCS 2006 and their impact on aerosol direct radiative forcing. J. Geophys. Res. Atmos. 114 https://doi.org/10.1029/2008JD011604.

Mikhailov, E., Vlasenko, S., Martin, S.T., Koop, T., Pöschl, U., 2009. Amorphous and crystalline aerosol particles interacting with water vapor: conceptual framework and experimental evidence for restructuring, phase transitions and kinetic limitations. Atmos. Chem. Phys. 9, 9491–9522. https://doi.org/10.5194/acp-9-9491-2009.

Martin, M., et al., 2013. Hygroscopic properties of fresh and aged wood burning particles. J. Aerosol Sci. 56, 15–29. https://doi.org/10.1016/j.jaerosci.2012.08.006.

McMurry, P.H., et al., 2005. A criterion for new particle formation in the sulfur-rich Atlanta atmosphere. J. Geophys. Res. Atmos. 110, D22S02. https://doi:10.1029/2005JD00590.

Ogulei, D., Hopke, P.K., Wallace, L.A., 2006. Analysis of indoor particle size distributions from an occupied townhouse using positive matrix factorization. Indoor Air 16, 204–215. https://doi.org/10.1111/j.1600-0668.2006.00418.x.

Petters, M.D., Kreidenweis, S.M., 2007. A single parameter representation of hygroscopic growth and cloud condensation nucleus activity. Atmos. Chem. Phys. 7, 1961–1971. https://doi.org/10.5194/acp-7-1961-2007.

Paatero, P., 1999. The multilinear engine - a table-driven, least squares program for solving multilinear problems, including the n-way parallel factor analysis model. J. Comput. Graph Stat. 8, 854–888. https://doi.org/10.2307/1390831.

Paatero, P., et al., 2014. Methods for estimating uncertainty in factor analytic solutions. Atmos. Meas. Tech. 7, 781–797. https://doi.org/10.5194/amt-7-781-2014.

Pey, J., et al., 2009. Source apportionment of urban fine and ultrafine particle number concentration in a western Mediterranean city. Atmos. Environ. 43, 4407–4415. https://doi.org/10.1016/j.atmosenv.2009.05.024.

Petäjä, T., et al., 2007. Sub-micron atmospheric aerosols in the surroundings of Marseille and Athens: physical characterization and new particle formation. Atmos. Chem. Phys. 7, 2705–2720. https://doi.org/10.5194/acp-7-2705-2007.

Qiu, Y., et al., 2019. Vertical characterization and source apportionment of water-soluble organic aerosol with high-resolution aerosol mass spectrometry in Beijing, China. ACS Earth Space Chem 3, 273–284. https://doi.org/10.1021/acsearthspacechem.8b00155.

Rosenfeld, D., et al., 2017. Inverse relations between amounts of air pollution and orographic precipitation. Science 315, 1396–1398. https://doi.org/10.1126/science.1137949.

Ren, J., et al., 2018. Using different assumptions of aerosol mixing state and chemical composition to predict CCN concentrations based on field measurements in urban Beijing. Atmos. Chem. Phys. 18, 6907–6921. https://doi.org/10.5194/acp-18-6907-2018.

Rose, D., et al., 2010. Cloud condensation nuclei in polluted air and biomass burning smoke near the mega-city Guangzhou, China – Part 1: size-resolved measurements and implications for the modeling of aerosol particle hygroscopicity and CCN activity. Atmos. Chem. Phys. 10, 3365–3383. https://doi.org/10.5194/acp-10-3365-2010.

Rissler, J., et al., 2005. Hygroscopic behaviour of aerosol particles emitted from biomass fired grate boilers. Aerosol Sci. Technol. 39, 919–930. https://doi.org/10.1080/02786820500331068.

Swietlicki, E., et al., 2008. Hygroscopic properties of submicrometer atmospheric aerosol particles measured with H-TDMA instruments in various environments – a review. Tellus B 60, 432–469. https://doi.org/10.1111/j.1600-0889.2008.00350.x.

Sakurai, H., et al., 2005. Hygroscopicity and volatility of 4–10 nm particles during summertime atmospheric nucleation events in urban Atlanta. J. Geophys. Res. Atmos. 110 https://doi.org/10.1029/2005JD005918.

Shingler, T., et al., 2016. Ambient observations of hygroscopic growth factor and f(RH) below 1: case studies from surface and airborne measurements. J. Geophys. Res. Atmos. 121 (13), 677, 661–13. https://doi:10.1002/2016JD025471.

Tritscher, T., et al., 2011. Changes of hygroscopicity and morphology during ageing of diesel soot. Environ. Res. Lett. 6 (3) https://doi.org/10.1088/1748-9326/6/3/034026.

Vu, T.V., Delgado-Saborit, J.M., Harrison, R.M., 2015. A review of hygroscopic growth factors of submicron aerosols from different sources and its implication for calculation of lung deposition efficiency of ambient aerosols. Air Qual. Atmos. Health. 8, 429–440. https://doi.org/10.1007/s11869-015-0365-0.

Vu, T.V., Shi, Z., Harrison, R.M., 2021. Estimation of hygroscopic growth properties of source-related sub-micrometre particle types in a mixed urban aerosol. NPJ Clim. Atmos. Sci. 4 https://doi.org/10.1038/s41612-021-00175-w.

Väkevä, M., Hämeri, K., Aalto, P., 2002a. Hygroscopic properties of nucleation mode and Aitken mode particles during nucleation bursts and in background air on the west coast of Ireland. J. Geophys. Res. Atmos. 107 (D19) https://doi.org/10.1029/2000JD000176.

Väkevä, M., Kulmala, M., Stratmann, F., Hämeri, K., 2002b. Field measurements of hygroscopic properties and state of mixing of nucleation mode particles. Atmos. Chem. Phys. 2, 55–66. https://doi.org/10.5194/acp-2-55-2002.

Wang, Y., Chen, Y., 2019. Significant climate impact of highly hygroscopic atmospheric aerosols in Delhi, India. Geophys. Res. Lett. 46, 5535–5545. https://doi.org/10.1029/2019GL082339.

Wu, Z.J., Poulain, L., et al., 2013. Relating particle hygroscopicity and CCN activity to chemical composition during the HCCT-2010 field campaign. Atmos. Chem. Phys. 13, 7983–7996. https://doi.org/10.5194/acp-13-7983-2013.

Wang, S.C., Flagan, R.C., 1990. Scanning electrical mobility spectrometer. Aerosol. Sci. Technol. 13, 230–240. https://doi.org/10.1080/02786829008959441.

Wu, Z.J., et al., 2016. Particle hygroscopicity and its link to chemical composition in the urban atmosphere of Beijing, China, during summertime. Atmos. Chem. Phys. 16 (2), 1123–1138. https://doi.org/10.5194/acp-16-1123-2016.

Wang, Y., et al., 2017. Enhanced hydrophobicity and volatility of submicron aerosols under severe emission control conditions in Beijing. Atmos. Chem. Phys. 17 (8), 5239–5251. https://doi.org/10.5194/acp-17-5239-2017.

Wang, Q., et al., 2015. Chemical composition of aerosol particles and light extinction apportionment before and during the heating season in Beijing, China. J. Geophys. Res. Atmos. 120 (24) https://doi.org/10.1002/2015JD023871, 12,708-712,722.

Wang, G., et al., 2016. Persistent sulfate formation from London Fog to Chinese haze. Proc. Natl. Acad. Sci. USA 113 (48), 13. https://doi.org/10.1073/pnas.1616540113, 630–13,635.

Wu, Z.J., et al., 2018. Aerosol liquid water driven by anthropogenic inorganic salts: implying its key role in haze formation over the North China Plain. Environ. Sci. Technol. Lett. 5 (3), 160–166. https://doi.org/10.1021/acs.estlett.8b00021.

Wu, Z., et al., 2017. Chemical and physical properties of biomass burning aerosols and their CCN activity: a case study in Beijing, China. Sci. Total Environ. 579, 1260–1268.

Wang, J., et al., 2010. The importance of aerosol mixing state and size-resolved composition on CCN concentration and the variation of the importance with atmospheric aging of aerosols. Atmos. Chem. Phys. 10 (15), 7267–7283. https://doi.org/10.5194/acp-10-7267-2010.

Xu, W., Kuang, Y., et al., 2020. Current challenges in visibility improvement in southern China. Environ. Sci. Technol. Lett. 7 (6), 395–401. https://doi.org/10.1021/acs.estlett.0c00274.

Xu, W., et al., 2019. Changes in aerosol chemistry from 2014 to 2016 in winter in Beijing: insights from high-resolution aerosol mass spectrometry. J. Geophys. Res. Atmos. 124 (2), 1132–1147. https://doi.org/10.1029/2018JD029245.

Zhao, G., Hu, M., et al., 2022. Current challenges in visibility improvement in Sichuan Basin. Geophys. Res. Lett. 49 (12), e2022GL098836 https://doi.org/10.1029/2022GL098836.

Zhang, F., et al., 2022. The effect of Black carbon aging from NO2 oxidation of SO2 on its morphology, optical and hygroscopic properties. Environ. Res. 212, 113238 https://doi.org/10.1016/j.envres.2022.113238.

Zhang, F., et al., 2017. Uncertainty in predicting CCN activity of aged and primary aerosols. J. Geophys. Res. Atmos. 122 (21), 11723–11736. https://doi.org/10.1002/2017JD027058.

Zhang, F., et al., 2019. Significantly enhanced aerosol CCN activity and number concentrations by nucleation-initiated haze events: a case study in urban Beijing. J. Geophys. Res. Atmos. 124 (24), 14. https://doi.org/10.1029/2019JD031457, 102–14,113.

Zhao, J., et al., 2017. Insights into aerosol chemistry during the 2015 China Victory Day parade: results from simultaneous measurements at ground level and 260 m in Beijing. Atmos. Chem. Phys. 17 (4), 3215–3232. https://doi.org/10.5194/acp-17-3215-2017.

Zhang, R., et al., 2004. Atmospheric new particle formation enhanced by organic acids. Science 304, 1487–1490. https://doi.org/10.1126/science.1095139.